

Novel Orbital Ordering Induced by Anisotropic Stress in a Manganite Thin Film

Y. Wakabayashi,¹ D. Bizen,² H. Nakao,² Y. Murakami,^{2,3} M. Nakamura,^{4,*} Y. Ogimoto,⁵ K. Miyano,⁶ and H. Sawa¹

¹Photon Factory, Institute of Materials Structure Science, High Energy Accelerator Research Organization, Tsukuba 305-0801, Japan

²Department of Physics, Tohoku University, Sendai 980-8578, Japan

³Synchrotron Radiation Research Center, JAERI, Sayo 679-5148, Japan

⁴Department of Applied Physics, University of Tokyo, Tokyo 113-8586, Japan

⁵Devices Technology Research Laboratories, SHARP Corporation, Nara 632-8567, Japan

⁶Research Center for Advanced Science and Technology, University of Tokyo, Tokyo 153-8904, Japan

(Received 15 June 2005; published 4 January 2006)

A novel structure of orbital ordering is found in a $\text{Nd}_{0.5}\text{Sr}_{0.5}\text{MnO}_3$ thin film, which exhibits a clear first-order transition, by synchrotron x-ray diffraction measurements. Lattice parameters vary drastically at the metal-insulator transition at 170 K ($= T_{\text{MI}}$), and superlattice reflections appear below 140 K ($= T_{\text{CO}}$). The electronic structure between T_{MI} and T_{CO} is identified as *A*-type antiferromagnetic with a $d_{x^2-y^2}$ ferro-orbital ordering. The new type of antiferro-orbital ordering characterized by the wave vector $(\frac{1}{4}\frac{1}{4}\frac{1}{2})$ in cubic notation emerges below T_{CO} . The accommodation of the large lattice distortion at the first-order phase transition and the appearance of the novel orbital ordering are brought about by the anisotropy in the substrate, a new parameter for the phase control.

DOI: 10.1103/PhysRevLett.96.017202

PACS numbers: 75.70.-i, 61.10.Nz, 75.47.Lx

Charge ordering and orbital ordering (CO-OO) are the characteristic phenomena that render the complex electronic phase behavior to the strongly correlated electron systems, manganites in particular [1]. A number of theoretical and experimental studies on CO-OO in $R_{1-x}A_x\text{MnO}_3$ (RE: rare earth metals; AE: alkali earth metals) have been conducted in the vicinity of $x = 0.5$ in order to understand the mechanism of the ordering and the resulting electronic properties [2]. Only three types of OO have been found dominant—one type of antiferro-orbital structure (staggered arrangement of $d_{3x^2-r^2}$ and $d_{3y^2-r^2}$ orbitals, *CE*-OO) corresponding to *CE*-type antiferromagnetism (AFM) and two types of ferro-orbital structures ($d_{3z^2-r^2}$ and $d_{x^2-y^2}$) corresponding to *C*-type and *A*-type AFM, respectively.

The orbital order couples intimately to the lattice distortion. One can easily envision that a tetragonal lattice distortion promotes ferro-orbital structures; the compressive strain within the *c* plane favors $d_{3z^2-r^2}$ (*C*-OO), while the tensile strain favors $d_{x^2-y^2}$ (*A*-OO). In fact, the phase control of ferro-orbital ordering was achieved by manipulating the tetragonal lattice parameters employing a thin-film technique fabricated on (001) substrates [3]. In contrast, the antiferro-orbital ordering inevitably involves the in-plane anisotropy, and no effective means for its control has been available thus far.

Thin manganite films on (011) substrates [4] were recently found to exhibit a variety of clear first-order phase transitions [5,6], which has not been possible in those on (001) substrates studied extensively [7–10]. From the transport and magnetic properties of these films, the antiferro-orbital order has been anticipated in them, although the direct evidence of the OO as well as the knowledge of the OO structures in these films, which affect

the magnetic and/or electronic properties, were lacking. In this Letter, we present results of synchrotron x-ray diffraction measurements on a $\text{Nd}_{0.5}\text{Sr}_{0.5}\text{MnO}_3$ thin film grown on $\text{SrTiO}_3(011)$. A novel antiferro-orbital structure has been identified. We clearly demonstrate a new handle to manipulate the OO, the *anisotropic stress*.

The x-ray diffraction experiment was carried out at BL-4C and BL-16A2 of the Photon Factory, KEK, Japan. The beam lines are equipped with standard four-circle diffractometers connected to closed-cycle refrigerators. Epitaxial films were grown by the pulsed laser deposition method [5,6]. The thickness of the sample was 80 nm. Figure 1 shows the temperature dependence of the resistivity of $\text{Nd}_{0.5}\text{Sr}_{0.5}\text{MnO}_3$ thin films grown on $\text{SrTiO}_3(001)$, (011), and (111) substrates along with that of bulk $\text{Nd}_{0.5}\text{Sr}_{0.5}\text{MnO}_3$. The film on the (011) substrate clearly shows the first-order insulator-metal phase transition while

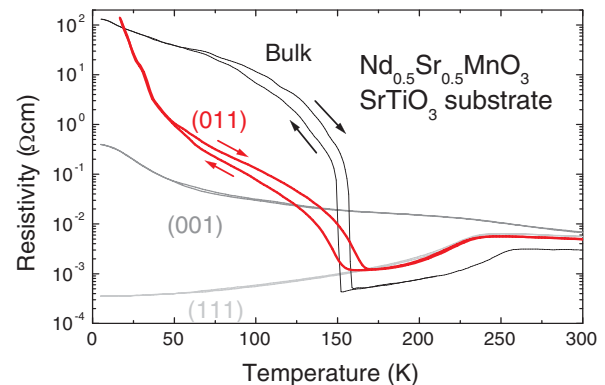


FIG. 1 (color online). Temperature dependence of the electric resistivity of $\text{Nd}_{0.5}\text{Sr}_{0.5}\text{MnO}_3$ thin films grown on $\text{SrTiO}_3(001)$, (011), and (111) substrates [6] and of bulk $\text{Nd}_{0.5}\text{Sr}_{0.5}\text{MnO}_3$ [20].

films on other substrates show only monotonous temperature dependence. The transition, however, is not as sharp as that in the bulk sample, and the temperature dependence of the resistivity is also different, which is shown below to be a signature of the new OO in the film. It should be noted that the electronic and magnetic properties show no essential thickness dependence [5].

First, we investigated the distortion in the primitive perovskite cell. A schematic view of the a^* plane in the reciprocal space is shown in Fig. 2(a). The lattice constants at room temperature are $a = 3.905 \text{ \AA}$, $b = c = 3.824 \text{ \AA}$, $\alpha = 90.5^\circ$, and $\beta = \gamma = 90.3^\circ$. As reported earlier [5,6], the lattice constant a is locked to the substrate, while that for $[0\bar{1}1]$ is unlocked. The (002) reflection splits into four peaks at 10 K, i.e., $(\pm 0.008, +0.028, 2 + 0.028)$ and $(\pm 0.008, -0.028, 2 - 0.028)$. The closed circles in Fig. 2(a) show a schematic view of the reciprocal lattice at 10 K. The split along the a^* direction is ignored as it is very small. The lattice parameters at 10 K are $a = 3.896 \text{ \AA}$, $b = 3.867 \text{ \AA}$, $c = 3.761 \text{ \AA}$, $\alpha = 90.4^\circ$, $\beta =$

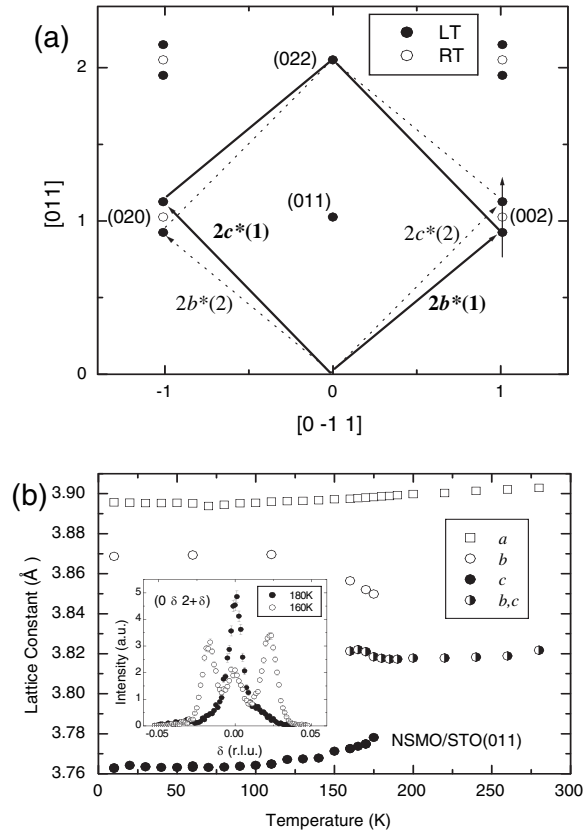


FIG. 2. (a) Schematic view of the a^* plane in reciprocal space at room temperature and 10 K. Twinning was observed at 10 K. (b) Temperature dependence of the lattice parameters a , b , and c during a heating run. The lattice parameter of SrTiO_3 is shown as a because a was locked into the lattice parameter of the substrate that can be measured precisely. The inset shows the peak profiles obtained at 180 and 160 K along the arrow through (002) shown in (a).

90.1° , and $\gamma = 90.6^\circ$. The temperature dependence of the lattice constants during a heating run is shown in Fig. 2(b). Lattice parameters b and c vary drastically at T_{MI} , while lattice parameter a , which is locked to the substrate, is almost constant. This freedom of lattice parameters allows the first-order transition where the resistivity rapidly changes; epitaxial films on (001) substrates are tetragonally locked, and this type of distortion is suppressed. The peak profiles of a (011) line passing through the (002) position at 160 and 180 K are shown in the inset of the figure. The profile at 160 K clearly shows the phase coexistence of high-temperature phase and, as shown later, A -OO phase. The lattice parameters observed are numerically similar to those of bulk crystals listed in Ref. [11] after the cell transformation to cubic notation, $a = b = 3.853 \text{ \AA}$ and $c = 3.812 \text{ \AA}$ at 300 K and $a = b = 3.872 \text{ \AA}$ and $c = 3.759 \text{ \AA}$ at 10 K, CE -OO phase; lattice constants in A -OO phase is nearly equal to those in CE -OO phase. In particular, the change in the lattice parameters below T_{MI} characterized by $a \approx b > c$ is in good agreement with that associated with A -OO or CE -OO. Therefore, the temperature dependence of the lattice parameters suggests that A -OO or CE -OO is established below T_{MI} .

Next, we searched for superlattice reflections corresponding to the orbital ordering in the region of $0.5 \leq h \leq 1$ and $1.5 \leq \{k, l\} \leq 2$. Superlattice reflections characterized by the wave vector $(\frac{1}{2} \frac{1}{2} \frac{1}{2})$ are observed at room temperature. These reflections are caused by the MnO_6 -octahedra rotation and the concomitant displacement of A -site (Nd and Sr) ions. At 10 K, the intensity of these reflections differs from that observed at room temperature, indicating that the magnitude of the MnO_6 -octahedra rotation changes with the phase transition. In addition, the superlattice reflections corresponding to the $\sqrt{2} \times 2\sqrt{2} \times 2$ superstructure were observed at this temperature. This size of the unit cell is the same as that of the bulk compounds exhibiting CE -OO.

Figure 3(a) shows the intensity distribution around several superlattice positions; the intensity was normalized so that the peak top of the (011) fundamental reflection is 10^6 . Clearly, some new peaks emerge at low temperature. The $(\frac{3}{4} \frac{7}{4} \frac{3}{2})$ peak characterized by the wave vector $(\frac{1}{4} \frac{1}{4} \frac{1}{2})$ was strong while the $(\frac{3}{4} \frac{7}{4} 2)$ peak characterized by $(\frac{1}{4} \frac{1}{4} 0)$ was not observed. The energy spectrum of $(\frac{1}{2} \frac{3}{2} 2)$ intensity is shown in the inset of Fig. 3(b). It shows a clear resonance feature at the Mn K-absorption edge, indicating that two or more nonequivalent Mn sites form a periodic arrangement with the wave vector $(\frac{1}{2} \frac{1}{2} 0)$, the ordinary charge ordering. The temperature dependence of the $(\frac{3}{4} \frac{7}{4} \frac{3}{2})$ and $(\frac{1}{2} \frac{3}{2} 2)$ intensity is shown in Fig. 3(b). The intensity of the two peaks has identical temperature dependence. The peaks appear at 140 K ($= T_{\text{CO}}$) during the cooling run. This temperature is significantly lower than T_{MI} at which the (002) reflection splits. We searched for superlattice reflections at 160 K, the temperature between T_{CO} and T_{MI} , and

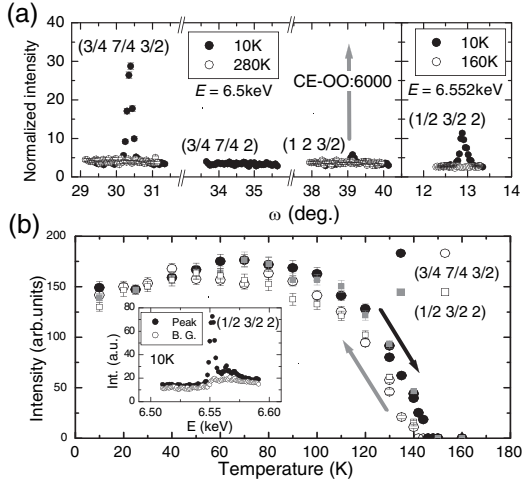


FIG. 3. (a) Intensity distribution around $(\frac{3}{4} \ \frac{7}{4} \ \frac{3}{2})$, $(\frac{3}{4} \ \frac{7}{4} \ 2)$, $(12 \ \frac{3}{2})$, and $(\frac{1}{2} \ \frac{3}{2} \ 2)$, which are characterized by the wave vectors $(\frac{1}{4} \ \frac{1}{4} \ \frac{1}{2})$, $(\frac{1}{4} \ \frac{1}{4} \ 0)$, $(00 \ \frac{1}{2})$, and $(\frac{1}{2} \ \frac{1}{2} \ 0)$, respectively; the intensity is normalized so that the peak top of the (011) fundamental reflection is 10^6 . Assuming the structure of $\text{La}_{0.5}\text{Ca}_{0.5}\text{MnO}_3$ having *CE*-OO [17], $(12 \ \frac{3}{2})$ intensity of 6000 is expected. (b) Temperature dependence of $(\frac{3}{4} \ \frac{7}{4} \ \frac{3}{2})$ (circles) and $(\frac{1}{2} \ \frac{3}{2} \ 2)$ (squares) intensity measured with incident x rays of 6.552 keV, *on-resonant* energy. The intensity of the latter is multiplied by a factor of 2.5 for presentation. The open and closed symbols correspond to the cooling and heating run, respectively. The inset shows the energy spectrum of the $(\frac{1}{2} \ \frac{3}{2} \ 2)$ reflection at 10 K.

found no peak except for the $(\frac{1}{2} \ \frac{1}{2} \ \frac{1}{2})$ reflections. The electronic state in this temperature region will be discussed later.

The superlattice reflections with the wave vector $(\frac{1}{4} \ \frac{1}{4} \ \frac{1}{2})$ observed at 10 K imply that the in-plane structure is the same as that of *CE*-OO with $(\frac{1}{4} \ \frac{1}{4} \ 0)$ diffraction. However, the stacking pattern alternates along the *c* direction. The regular *CE*-OO structure is shown in Fig. 4(a). The in-plane orbital arrangement is common to systems having a variety of structure types, i.e., single-layered [12], bilayered [13], and A-site ordered manganites [14–16], while the stacking vectors are different. Therefore, it is reasonable to expect that our film has also the same in-plane orbital arrangement. Under this assumption, we arrive at a unique solution of the orbital arrangement in the film. The result is shown in Fig. 4(b). We term this arrangement antiphase-OO (*AP*-OO). We can distinguish *CE*-OO and *AP*-OO by measuring $(12 \ \frac{3}{2})$ peak, which is mainly caused by the displacement of A-site ions, shown in Fig. 3(a). In the *CE*-OO, A-site ions are sandwiched between MnO_2 sheets with the same staggered orbital arrangement above and below, while in the *AP*-OO, the orbital arrangements above and below are out of phase. Assuming that Mn ions are located on the corners of a cube, it can easily be shown that the center of the cube is the center of inversion for the charge distribution of Mn and O ions in the *AP*-OO while it is not in the *CE*-OO. Because of the electrostatic stress, the

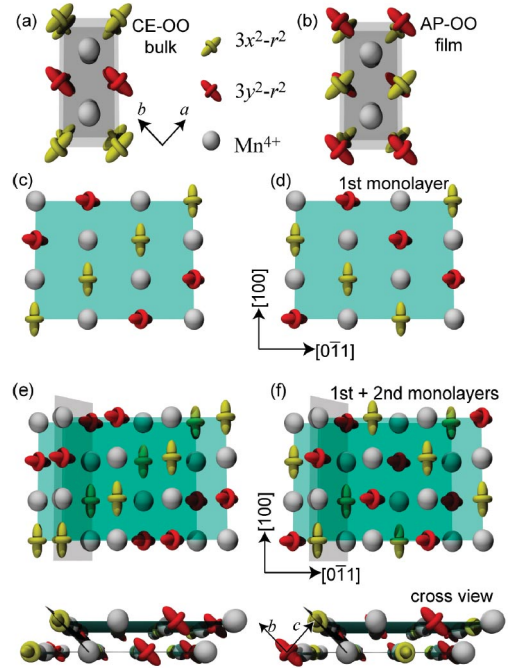


FIG. 4 (color). (a) Schematic view of the orbital arrangement of *CE*-OO (bulk structure). The Mn^{4+} ions are indicated by white spheres, while Mn^{3+} ions with the $3x^2 - r^2$ ($3y^2 - r^2$) orbital are indicated by yellow (red) symbols. (b) The same as (a) but for the *AP*-OO (film structure). (c) The orbital arrangement of the first monolayer with *CE*-OO on the (011) substrate observed from the [011] direction. (d) That for *AP*-OO. (e) The same as (c) but for the first two monolayers. Bottom figure shows the view from the $[\bar{1}00]$ direction. The [011] planes, which are parallel to the surface of the substrate, and the [001] planes are represented by green and gray transparent plates, respectively. (f) That for *AP*-OO.

A-site ions in the *CE*-OO are displaced from the center of the hexahedron formed by the nearest neighbor Mn ions as is observed experimentally. Based on the structural data of $\text{La}_{0.5}\text{Ca}_{0.5}\text{MnO}_3$ crystal in the *CE*-OO phase [17], the intensity of the $(12 \ \frac{3}{2})$ peak is calculated to be as strong as 0.6% of the (011) fundamental reflection intensity with the peak splitting at low temperatures taken into account. In contrast, the A-site ions are expected to be near the center in the *AP*-OO, and hence little intensity at $(12 \ \frac{3}{2})$ should result, which is indeed the case as shown in Fig. 3(a). We therefore concluded that the *AP*-OO is established. The observed lattice parameters ($a \approx b > c$) are similar to those of *CE*-OO and A-OO in bulk crystals because the e_g electrons in these three OO structures distribute in the *c* plane.

It should be noted that the *AP*-OO must carry a magnetic structure different from that of *CE*-OO. The magnetic structure of the *AP*-OO state in the *c* plane must be the same as that of the *CE*-AFM, i.e., the antiferromagnetic arrangement of zigzag ferromagnetic chains resulting from the anisotropic ferromagnetic interaction of ordered e_g

orbitals. The stacking structure in the *CE*-AFM is antiferromagnetic. In contrast, perfect antiferromagnetic stacking is impossible in the *AP*-OO because of the shift of the phase in the zigzag chains in the neighboring planes. Under this constraint, two types of stacking structures are possible: the neighboring Mn^{3+} spins in the *c* direction are parallel and Mn^{4+} spins antiparallel or vice versa. In both cases, lines of interplane transfer thread through the *c* planes resulting in a unique network structure. This structure is consistent with nearly isotropic but slightly enhanced electric conductivity in the $[0\bar{1}1]$ direction [5].

The *AP*-OO has not been observed in the bulk compounds thus far. The novel orbital arrangement is evidently stabilized by the strain from the substrate. For a given zigzag pattern in the *c* plane, the orbital arrangement within a $[011]$ plane in *CE*-OO and that in the *AP*-OO are identical except for the rotation of 180° about the *a* axis. This is shown in Figs. 4(c) and 4(d), which indicate the first monolayers on the SrTiO_3 (011) substrates. Thus, the energy difference must come from the effect of the second monolayer. The second layer structures are shown in Figs. 4(e) and 4(f). For *CE*-OO, the stress exerted by the film on the substrate is nonuniform, because the locally distorted primitive perovskite cells stack up in phase. On the other hand, the stress in the *AP*-OO is evenly distributed within the $[011]$ plane since the arrangement is staggered. This difference can produce the energy gain of the *AP*-OO arrangement. It should be stressed that a uniquely defined crystallographic axis, as is demonstrated here, is of great importance for the study of macroscopic anisotropic properties and can rarely be achieved in bulk single crystals [18].

The stacking structure of the orbital ordering may also be affected by the distortion of the *A*-site ions through the hybridization of *A*-site ions and oxygens [19]. Since the unit cells of the film are strained by the substrate, the magnitude of the displacement of the *A*-site ions should differ from that of the bulk compound. This may change the stacking structure of the orbitals. However, detailed theoretical calculations of some orbital arrangements as a function of the *A*-site displacement has been carried out only for $x = 0$ [19]. Theoretical attention for $x = 0.5$ is needed for detailed analysis.

Finally, we discuss the electronic state of the film between T_{CO} and T_{MI} where the film has a significantly smaller *c*-lattice parameter than the other two and no superlattice reflection. The small *c* is the characteristic of *CE*-OO, *AP*-OO, and *A*-OO. However, *CE*-OO and *AP*-OO should produce the superlattice reflections characterized by the wave vectors $(\frac{1}{4}\frac{1}{4}0)$ and $(\frac{1}{4}\frac{1}{4}\frac{1}{2})$, which are not observed in this temperature range. Therefore, the expected orbital state is *A*-OO. Since magnetism is closely related to the orbital state, the suppression of the spontaneous magnetization below T_{MI} (the *A*-type antiferromagnetic state) [5,6] is a natural consequence. The occurrence

of *A*-type AFM in this film is not surprising because the free energy of the *A*-type AFM is similar to that of *CE*-OO, and thus that of *AP*-OO for the $\text{Nd}_{1-x}\text{Sr}_x\text{MnO}_3$ system. In fact, the bulk compound with $x = 0.51$ exhibits the *A*-type AFM below 200 K [11].

In summary, a new type of orbital ordering was observed in a thin film of $\text{Nd}_{0.5}\text{Sr}_{0.5}\text{MnO}_3$ fabricated on a SrTiO_3 (011) substrate. The orbital arrangement is clarified and the formation mechanism of this new orbital structure is discussed. The temperature dependence of the lattice parameters and the orbital ordered state are determined. *A*-type AFM/ $d_{x^2-y^2}$ ferro-orbital order also appears at the intermediate temperature region. These results clearly show that various orbital structures can be realized in thin films, including the ones that do not appear in the bulk crystal. The anisotropic stress from the substrate is a new parameter for controlling the electronic state in addition to the ionic radii and the hole concentration.

The authors are grateful to Professor T. Arima and Dr. J. P. Hill for fruitful discussions. This work was supported by a Grant-in-Aid for Creative Scientific Research (13NP0201), TOKUTEI (16076207) from the Ministry of Education, Culture, Sports, Science and Technology of Japan, and JSPS KAKENHI (15104006). Financial support to M.N. by the 21st Century COE Program for ‘‘Applied Physics on Strong Correlation’’ administered by Department of Applied Physics, The University of Tokyo, is also appreciated.

*Present address: Correlated Electron Research Center (CERC), National Institute of Advanced Industrial Science and Technology (AIST), Tsukuba, Ibaraki 305-8562, Japan.

- [1] Y. Tokura and N. Nagaosa, *Science* **288**, 462 (2000).
- [2] Z. Fang *et al.*, *Phys. Rev. Lett.* **84**, 3169 (2000).
- [3] Y. Konishi *et al.*, *J. Phys. Soc. Jpn.* **68**, 3790 (1999).
- [4] Note that the notation of the crystallographic axes is different from earlier reports [5,6].
- [5] Y. Ogimoto *et al.*, *Phys. Rev. B* **71**, 060403(R) (2005).
- [6] M. Nakamura *et al.*, *Appl. Phys. Lett.* **86**, 182504 (2005).
- [7] W. Prellier *et al.*, *Phys. Rev. B* **62**, R16337 (2000).
- [8] Y. Ogimoto *et al.*, *Appl. Phys. Lett.* **78**, 3505 (2001).
- [9] A. Biswas *et al.*, *Phys. Rev. B* **63**, 184424 (2001).
- [10] E. R. Buzin *et al.*, *Appl. Phys. Lett.* **79**, 647 (2001).
- [11] R. Kajimoto *et al.*, *Phys. Rev. B* **60**, 9506 (1999).
- [12] Y. Murakami *et al.*, *Phys. Rev. Lett.* **80**, 1932 (1998).
- [13] D. N. Argyriou *et al.*, *Phys. Rev. B* **61**, 15269 (2000).
- [14] M. Uchida *et al.*, *J. Phys. Soc. Jpn.* **71**, 2605 (2002).
- [15] T. Arima *et al.*, *Phys. Rev. B* **66**, 140408(R) (2002).
- [16] H. Gageyama *et al.*, *J. Phys. Soc. Jpn.* **72**, 241 (2003).
- [17] P. G. Radaelli *et al.*, *Phys. Rev. B* **55**, 3015 (1997).
- [18] K. Tobe, T. Kimura, and Y. Tokura, *Phys. Rev. B* **69**, 014407 (2004).
- [19] T. Mizokawa *et al.*, *Phys. Rev. B* **60**, 7309 (1999).
- [20] Y. Tokura *et al.*, *Phys. Rev. Lett.* **76**, 3184 (1996).